Journal of the American Heart Association

ORIGINAL RESEARCH

Pressure Overload Greatly Promotes Neonatal Right Ventricular Cardiomyocyte Proliferation: A New Model for the Study of Heart Regeneration

Lincai Ye, MD, PhD*; Shoubao Wang, MD*; Yingying Xiao, MS*; Chuan Jiang, MS; Yanhui Huang, MD; Huiwen Chen, MD; Haibo Zhang, MD; Hao Zhang, MD; Jinfen Liu, MD; Zhuoming Xu, MD, PhD; Haifa Hong, MD

BACKGROUND: Current mammalian models for heart regeneration research are limited to neonatal apex amputation and myocardial infarction, both of which are controversial. RNAseq has demonstrated a very limited set of differentially expressed genes between sham and operated hearts in myocardial infarction models. Here, we investigated in rats whether pressure overload in the right ventricle, a common phenomenon in children with congenital heart disease, could be used as a better animal model for heart regeneration studies when considering cardiomyocyte proliferation as the most important index.

METHODS AND RESULTS: In the rat model, pressure overload was induced by pulmonary artery banding on postnatal day 1 and confirmed by echocardiography and hemodynamic measurements at postnatal day 7. RNA sequencing analyses of purified right ventricular cardiomyocytes at postnatal day 7 from pulmonary artery banding and sham-operated rats revealed that there were 5469 differentially expressed genes between these 2 groups. Gene ontology and Kyoto Encyclopedia of Genes and Genomes analysis showed that these genes mainly mediated mitosis and cell division. Cell proliferation assays indicated a continuous overproliferation of cardiomyocytes in the right ventricle after pulmonary artery banding, in particular for the first 3 postnatal days. We also validated the model using samples from overloaded right ventricles of human patients. There was an approximately 2-fold increase of Ki67/pHH3/aurora B-positive cardiomyocytes in human-overloaded right ventricles compared with nonoverloaded right ventricles. Other features of this animal model included cardiomyocyte hypotrophy with no fibrosis.

CONCLUSIONS: Pressure overload profoundly promotes cardiomyocyte proliferation in the neonatal stage in both rats and human beings. This activates a regeneration-specific gene program and may offer an alternative animal model for heart regeneration research.

Key Words: cardiomyocyte ■ pressure overload ■ proliferation ■ right ventricle ■ RNA-seq

Heart failure (HF) is a leading cause of death, and an estimated 26 million people have HF worldwide.[1] HF ranks as the highest healthcare expense in China.[2] Stimulating pre-existing cardiomyocytes to proliferate and replace unhealthy or damaged cardiomyocytes after myocardial infarction or other trauma is a fundamental part of treating HF.[3] However, current mammalian models for heart regeneration research are limited to neonatal apex amputation and myocardial infarction, both of which are rarely observed in human infants, so it is difficult to find matched human infant samples to study regeneration. There are many

Correspondence to: Haifa Hong, MD and Zhuoming Xu, MD, PhD, Department of Thoracic and Cardiovascular Surgery, Shanghai Children's Medical Center, Shanghai Jiaotong University School of Medicine, 1678 Dongfang Rd, Shanghai 200127, China. E-mail: hhfsmallboat@163.com, zmxyfb@163.com

Supplementary Materials for this article are available at https://www.ahajournals.org/doi/suppl/10.1161/JAHA.119.015574

*Dr Ye, Dr Wang, and Miss Xiao contributed equally to this work and are co–first authors.

For Sources of Funding and Disclosures, see page 13.

JAHA is available at: www.ahajournals.org/journal/jaha

CLINICAL PERSPECTIVE

What Is New?

- Pressure overload, activating a regeneration-specific gene program, profoundly promotes cardiomyocyte proliferation in the neonatal stage in both rats and human beings.

What Are the Clinical Implications?

- When considering cardiomyocyte proliferation as the most important index, the pressure overload model could be a better animal model for heart regeneration studies than neonatal apex amputation and myocardial infarction models.

Nonstandard Abbreviations and Acronyms

GO	gene ontology
HF	heart failure
KEGG	Kyoto Encyclopedia of Genes and Genomes
PA	pulmonary artery
PAB	pulmonary artery banding
pHH3	phospho-histone H3
RNA-seq	RNA sequencing
RVCM	right ventricular cardiomyocyte
RV	right ventricle

inconsistent reports on these 2 models when considering regeneration: some authors have reported there is regeneration, while others have reported there is not regeneration.[4–10] Moreover, RNA sequencing (RNA-seq) transcriptome analysis has demonstrated only a very limited differential expression of genes between neonatal heart tissue with myocardial infarction and sham-operated heart tissue,[11] bringing into question whether a myocardial infarction model is really suitable for the study of heart regeneration.[7,10]

Pressure load is a key factor during fetal heart development. Without pressure load, the growth of the myocardium and heart size will be diminished.[12] During the neonatal stage, pressure overload also increases left ventricular cardiomyocyte proliferation, which protects the heart from maladaptation.[13] However, in clinical practice, pressure overload in the right ventricle (RV) is more common than in the left ventricle in children with congenital heart disease, such as tetralogy of Fallot, pulmonary artery hypertension, and pulmonary stenosis.[14–16] Whether pressure overload promotes right ventricular cardiomyocyte proliferation is unknown. If pressure overload contributes to both left and right ventricular cardiomyocyte proliferation at the neonatal stage, it is possible that it may contribute to prenatal cardiomyocyte proliferation. Pressure load to ventricle tissue at the late prenatal stage may be applied to rescue the tissue from dysplasia. Minimally invasive fetal surgery, which is increasingly common for lung and other diseases,[17] may also serve to rescue ventricular tissue from dysplasia, which otherwise generally requires heart transplantation after birth.[18]

An important issue is the differences between the left ventricles and RVs. The RV is different from the left ventricle in its anatomic, electrical, and cellular configuration.[19] More importantly, the pressures are different, which may impact the stiffness needed to handle wall pressure.[19] The RV often fails because of distinct pathobiological pathways that are separate from those of the left ventricle and therapy that influences the left ventricle favorably may not impact a dysfunctional RV.[20] Therefore, understanding whether pressure overload contributes to RV cardiomyocyte proliferation may be of benefit to the treatment of right ventricular failure.

Based on our previously described original right ventricular pressure overloaded rat model,[21] we performed RNA-seq to find out whether and how pressure overload can contribute to right ventricular cardiomyocyte proliferation. Also based on our previous publication and on the work of Polizzotti et al showing that human cardiomyocytes have a therapeutic/proliferation window,[22,23] we selected pressure overload of a human heart sample, age <3 months old, to verify the RNA-seq results.

MATERIALS AND METHODS

Data generated in this study are available from the corresponding author upon reasonable request. All of the RNA-seq data has been deposited in the GEO database (https://www.ncbi.nlm.nih.gov/geo) with accession number GSE139561.

All primers, reagents, and antibodies information are provided in Tables S1 through S3.

Animal Experiments

Pregnant Sprague–Dawley rats were purchased from Xipu'er-bikai Experimental Animal Co., Ltd (Shanghai, China). After birth, the rat neonates (both males and females) were randomized into 2 groups: an experimental group (PAB group), and a control group (sham group) that underwent the same procedure except for the banding step. Pulmonary artery banding (PAB) surgery was performed according to our previous publication.[21] Briefly, after neonatal rats were anesthetized by ice cooling, they were transferred to an ice bed and

fixed in the supine position. Horizontal thoracotomy was performed to reveal the pulmonary artery (PA). An 11-0 nylon thread was positioned under the PA, and a 30-gauge needle (0.31-mm diameter) was placed on the PA. The PA and needle were then tied together by the thread. We then removed the needle to form a fixed, constricted opening in the PA lumen. We closed the thoracic wall and then warmed the neonatal rats with a heat plate until natural movements and a red/pink complexion were achieved. We have provided a surgical video of our right ventricular overload model on a website [21] to enable others to learn the technique. All of the procedures conformed to the principles outlined in the Declaration of Helsinki and were approved by the Animal Welfare and Human Studies Committee at Shanghai Children's Medical Center.

Transthoracic Echocardiography

Rats were anesthetized with isoflurane and allowed to breathe spontaneously through a nasal cone (isoflurane/oxygen: 1.5%–2.0% maintenance). Echocardiograms were analyzed with a Vevo 2100 imaging system (Visual Sonics, Toronto, Ontario, Canada), and a long-axis view of the PA was used to measure the peak pressure gradient across the PA constriction by continuous-wave Doppler.

Histology

Postnatal day 7 (P7) rat hearts were fixed in 4% paraformaldehyde overnight at 4°C, then dehydrated in an ethanol series, embedded in paraffin, and sectioned into 6-μm slices. Hematoxylin and eosin staining was performed.

Cardiomyocyte Isolation and Purification

At P7, the young rats were decapitated. The hearts were carefully taken from the chest, and cardiomyocytes were dissociated by Langendorff reverse coronary perfusion with 200 μg/mL Liberase DH (Roche), as described elsewhere.[9] Cardiomyocytes were enriched by differential adherence and low-speed centrifugation.[24] The purity of cardiomyocytes was confirmed by flow cytometry. The purified cardiomyocytes were used for total RNA preparation and RNA-seq.

Total RNA Preparation and Real-Time Quantitative PCR Analysis

For mRNA quantification, mRNA was extracted and purified using a PureLink RNA Micro Scale Kit (Catalog No. 12183016; Life Technologies, Carlsbad, CA). RT-PCR was performed using the PrimeScript™ reagent kit (Takara Bio, Kusatsu, Japan). Quantitative real-time polymerase chain reaction (qRT-PCR) were carried out using SYBR Green Power Premix Kits (Applied Biosystems, Foster City, CA) according to the manufacturer's instructions. qRT-PCR was performed with a 7900 Fast Real-Time PCR System (Applied Biosystems), and the following conditions were used: 1 cycle at 95°C for 10 s, followed by 40 cycles of 95°C for 15 s and 60°C for 60 s. The primers were obtained from Generay Biotech Co., Ltd (Shanghai, China). The relative fold change was then calculated using the ΔΔCT method.

Library Preparation for Transcriptome Sequencing

A total amount of 1 μg RNA per sample was used as input material for the RNA sample preparations. Sequencing libraries were generated using the NEBNext® Ultra™ RNA Library Prep Kit for Illumina® (NEB, USA) following the manufacturer's recommendations. Index codes were added to attribute sequences to each sample. Briefly, mRNA was purified from total RNA using poly-T oligo-attached magnetic beads. Fragmentation was carried out using divalent cations under elevated temperature in NEB Next First Strand Synthesis Reaction Buffer (5×). First strand cDNA was synthesized using random hexamer primers and M-MuLV Reverse Transcriptase (RNase H –). Second strand cDNA synthesis was subsequently performed using DNA polymerase I and RNase H. Remaining overhangs were converted into blunt ends via exonuclease/polymerase activities. After adenylation of the 3′ ends of the DNA fragments, NEBNext Adaptors with hairpin loop structures were ligated to prepare for hybridization. In order to select cDNA fragments of preferentially 250–300 bp in length, the library fragments were purified with the AMPure XP system (Beckman Coulter, Beverly, MA). Then 3 μL USER Enzyme (NEB, USA) was used with size-selected, adaptor-ligated cDNA at 37°C for 15 minutes followed by 5 minutes at 95°C. Then, PCR was performed with Phusion High-Fidelity DNA polymerase, Universal PCR primers, and Index (X) Primer. At last, PCR products were purified (AMPure XP system), and library quality was assessed on an Agilent Bioanalyzer 2100 system.

Clustering and Sequencing

The clustering of the index-coded samples was performed on a cBot Cluster Generation System using a TruSeq PE Cluster Kit v3-cBot-HS (Illumina) according to the manufacturer's instructions. After cluster generation, the library preparations were sequenced on an Illumina Novaseq platform, and 150 bp paired-end reads were generated.

Quality Control, Read Mapping, and Quantification of Gene Expression Levels

Raw data (raw reads) in fastq format were first processed through in-house Perl scripts. In this step,

clean data (clean reads) were obtained by removing reads containing adapters, reads containing poly-N, and low-quality reads from raw data. At the same time, Q20, Q30, and GC content of the clean data were calculated. All of the downstream analyses were based on the clean data with high quality.

Reference genome and gene model annotation files were downloaded from the genome website directly. The index of the reference genome was built using Hisat2 v2.0.5, and paired-end clean reads were also aligned to the reference genome using Hisat2 v2.0.5. We selected Hisat2 as the mapping tool since it can generate a database of splice junctions based on the gene model annotation file and thus a better mapping result than other nonsplice mapping tools.

The expected number of fragments per kilobase of transcript sequence per million base pairs sequenced considers the effect of sequencing depth and gene length for the reads counted at the same time. Fragments per kilobase of transcript sequence per million is currently the most commonly used method for estimating gene expression levels. For this, featureCounts v1.5.0-p3 was used to count the number of reads mapped to each gene. Then, fragments per kilobase of transcript sequence per million of each gene was calculated based on the length of the gene and read counts mapped to each gene.

Differential Expression Analysis and Gene Ontology and Kyoto Encyclopedia of Genes and Genomes Enrichment Analysis of Differentially Expressed Genes

Differential expression analysis was performed using the DESeq2 R package (1.16.1). DESeq2 provides statistical routines for determining differential expression in digital gene expression data using a model based on the negative binomial distribution. The resulting *P* values were adjusted using Benjamini and Hochberg's approach for controlling the false discovery rate. Genes with an adjusted *P* value of <0.05 found by DESeq2 were assigned as differentially expressed.

Gene Ontology (GO) enrichment analysis of differentially expressed genes was implemented by the clusterProfiler R package, in which gene length bias was corrected. GO terms with corrected *P* values <0.05 considered to be significantly enriched by differentially expressed genes.

Kyoto Encyclopedia of Genes and Genomes (KEGG) is a database resource for understanding high-level functions and utilities of biological systems, such as the cell, the organism, and the ecosystem, from molecular-level information, especially large-scale molecular data sets generated by genome sequencing and other high-throughput experimental technologies (http://www.genome.jp/kegg/). We used the clusterProfiler R package to test the statistical enrichment of differentially expressed genes in KEGG pathways.

Tetralogy of Fallot Patients

We collected 20 right-ventricular-outflow myocardial tissue specimens from resections required to relieve obstructions in tetralogy of Fallot (TOF) patients at the Shanghai Children's Medical Center, Shanghai, China, between February 2015 and July 2018. Each specimen was preserved in liquid nitrogen and later divided into 3 portions, which were used for DNA extraction, qRT-PCR, and immunofluorescence. All of the procedures conformed to the principles outlined in the Declaration of Helsinki and were approved by the Animal Welfare and Human Studies Committee at the Shanghai Children's Medical Center. Parental written informed consent was obtained before study initiation.

Immunofluorescence

Slides were washed 3 times with PBS, fixed with 4% paraformaldehyde for 10 minutes, permeated with 0.5% Triton X-100 for 15 minutes, blocked with 10% donkey serum for 30 minutes, and stained with primary antibodies overnight at 4°C. After washing the slides 3 more times, we incubated the sections or cells with secondary antibodies and 4′,6-diamidino-2-phenylindole for 30 minutes. Three researchers who were blinded to sample identity quantified cellular Ki67, phospho-histone H3 (pH3), and aurora B via either manual counting or digital thresholding. This included image segmentation and creation of a binary image from a grayscale. We analyzed the converted binary images using ImageJ software (NIH, Bethesda, MD; Laboratory for Optical and Computational Instrumentation, University of Wisconsin, Madison, WI).

EdU Labeling

For EdU labeling experiments, rats were injected subcutaneously with 5 μg/g EdU at 24 hours before harvesting and signals were detected with a Click-iT@ Imaging Kit according to the manufacturer's instructions.

Statistical Analysis

Continuous data, including mRNA expression, protein expression, and number of Ki67/pH3/aurora B-positive cells, were expressed as means±SD. Differences were tested with Student *t* test if the data were normally distributed, otherwise they were tested with the rank sum test. *P* values <0.05 were considered to be statistically significant. Statistical analyses were performed using SAS software version 9.2 (SAS Institute Inc., Cary, NC).

RESULTS

Right Ventricular Pressure Load Is Significantly Increased in PAB Rats

To investigate whether pressure overload affects the proliferation of neonatal RV cardiomyocytes, first we constructed a RV pressure overload model by PAB in postnatal day 1(P1) rats. Most of the animals died in the first 2 days after surgery from P1 to P28. We thought the death may have been related to surgery. The survival rate was >75% on P28. After P28, most of them showed severe symptoms of right HF, such as cyanosis, ascites, and increased breathing rate, and they also began dying. We observed the rats up to 6 months, with one third left, which were euthanized. The autopsy showed the thrombosis in the femoral vein and significant right ventricular hypertrophy. Relative to the sham group, the peak pressure gradients across the PA constriction were significantly increased in the PAB group on P7 (Figure 1A and 1B). Consistently, histological examination showed that the RV free wall was significantly hypertrophic in the PAB group (n=6, *P*=0.0017, Figure 1C through E).Because of the increase of RV pressure, the septum moved toward the left ventricle (Figure 1C) These results suggested that RV pressure overload was successfully constructed as we previous showed.[21]

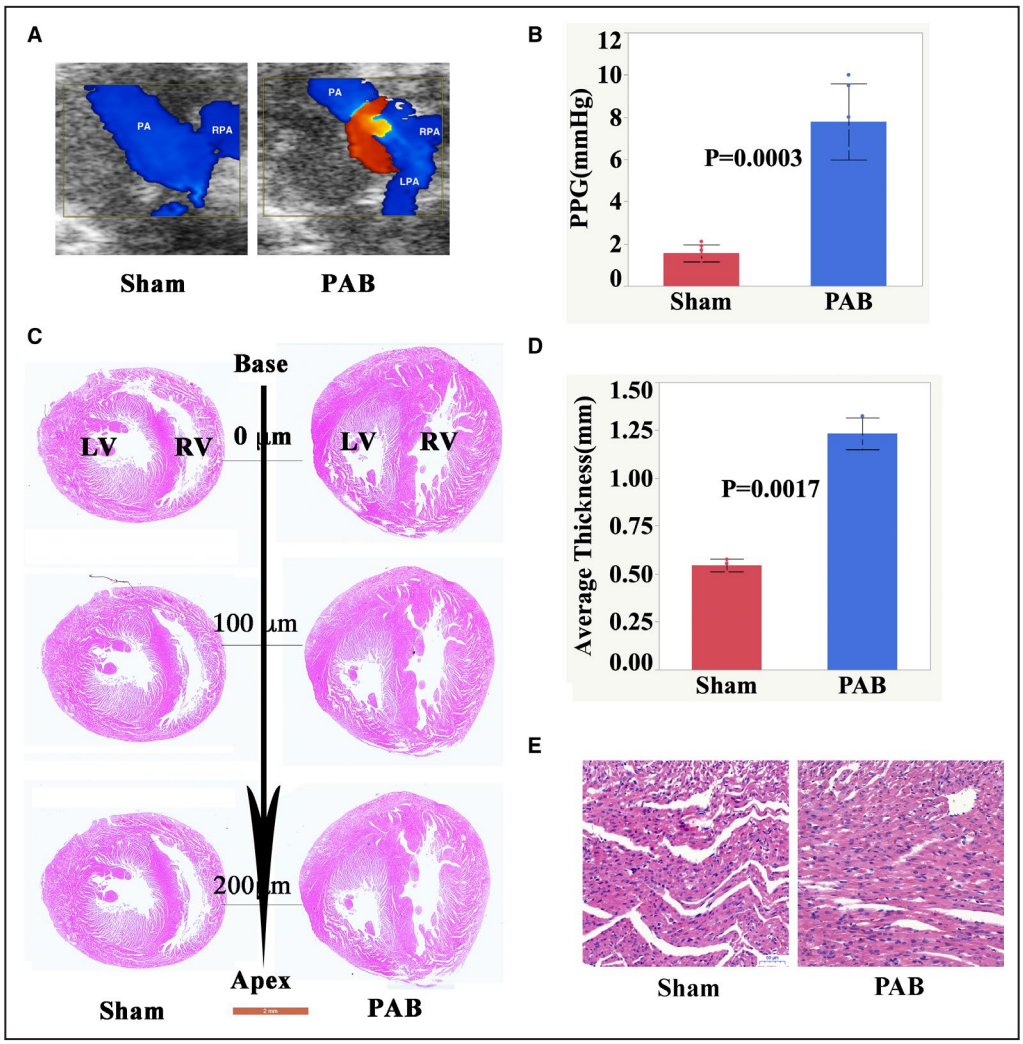

Figure 1. Establishment of right ventricular pressure overload model.
A, Representative echocardiographic images at P7 after sham and PAB surgery in neonatal rats. **B**, Graphical comparison of the PPG across PA constriction measured by transthoracic echocardiography between the sham and PAB groups. Data are presented as means±SD. Statistical analysis was performed using 2-tailed Student *t* tests. **C**, H&E-stained 2-chamber cross sections of a P7 heart (Scale bar: 2 mm). **D**, High magnification of H&E-stained sections of P7 RV. **E**, High magnification of H&E-stained sections of P7 right ventricle (Scale bar: 50 μm). H&E indicates hematoxylin and eosin; LPA, left pulmonary artery; LV, left ventricle; PA, pulmonary artery; PAB, pulmonary artery banding; PPG, peak pressure gradient; RPA, right pulmonary artery; and RV, right ventricle.

Pressure Overload Greatly Changes Genes Expression in Neonatal Right Ventricular Cardiomyocytes

To investigate how pressure overload changes gene expression in right ventricular cardiomyocytes (RVCMs), we isolated and purified cardiomyocytes from the RVs of the hearts of PAB and sham-operated mice (Figure S1) and performed RNA-seq on these cardiomyocytes. We verified the RNA-seq results by qRT-PCR (Figures S2 and S3) and have provided the list of top 24 genes and their detailed information (Figure S2 and Table S4). Our results showed that there were 5469 differentially expressed genes, among which 2567 were downregulated and 2902 were upregulated (Figure 2A). These 2 groups of cardiomyocytes shared

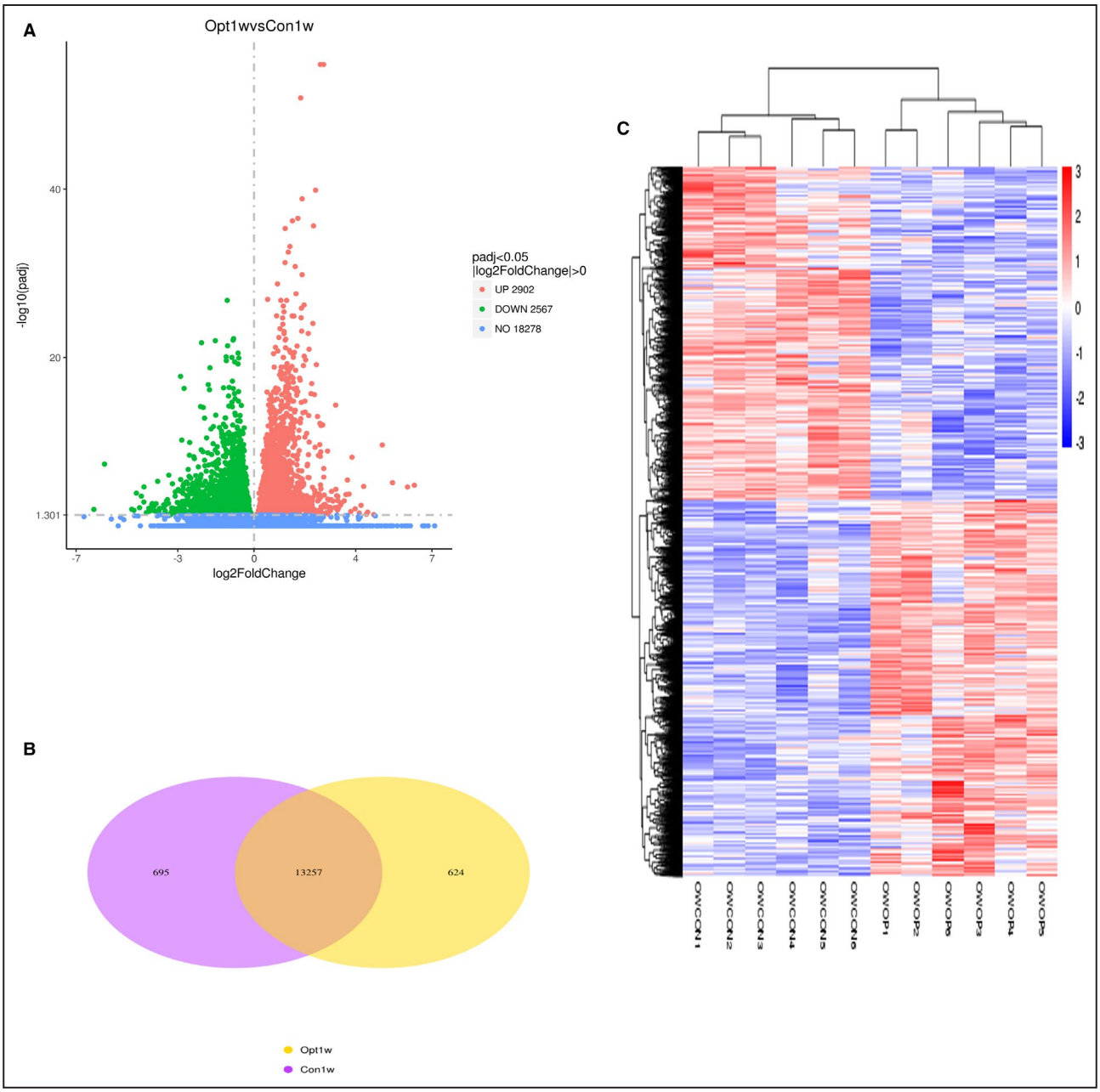

Figure 2. Pressure overload greatly changes gene expression of cardiomyocytes.
A, Volcano map of differentially expressed genes. There were 5469 differentially expressed genes between PAB (Operation-1 week, Opt1w) and sham (control-1 week, Con1w) groups, among which, 2902 genes were upregulated, and 2567 genes were downregulated. **B**, Venn diagram of differentially expressed genes. There were 13 257 genes expressed in both groups, 624 genes expressed only in the PAB group, and 695 genes expressed only in the sham group. **C**, Cluster analysis of differentially expressed genes. Every group had 6 rats. The clusters of genes in each animal in the same group were similar to each other but quite different from the other group. OWOP is from the PAB group; OWCON is from the sham group. OWCON indicates Operationer Wang-Control; OWOP, Operationer Wang-operationl; and PAB, pulmonary artery banding.

13 257 expressed genes in common. In the PAB group, another 624 genes were expressed (operation1week, opt1w), and 695 genes were expressed only in the sham group (control1week, con1w) (Figure 2B). When these genes were clustered, a heatmap showed that the individual rats in the same group were similar to each other but were noticeably different from the rats in the other group (Figure 2C).

Most Enriched GO Terms Are Closely Related to Cell Proliferation

We performed GO analysis to find out whether the differentially expressed genes were associated with cell proliferation. Biological process analysis showed that the top 10 most enriched GO terms were chromosome segregation, sister chromatid segregation, mitotic sister chromatid segregation, nuclear chromosome segregation, DNA replication, DNA repair, DNA-dependent DNA replication, regulation of cell cycle process, mitotic nuclear division, and organelle fission (Figure 3A through C). Cell component analysis showed the top 10 most enriched GO terms were chromosomal region, kinetochore, condensed chromosome-centromeric region, condensed chromosome kinetochore, condensed chromosome, spindle, centrosome, condensed chromosome outer kinetochore, and condensed nuclear chromosome kinetochore (Figure 3A through D). Molecular function analysis showed the top 10 most enriched GO terms were DNA-dependent ATPase activity, catalytic activity acting on DNA, histone binding, ATP-dependent DNA helicase activity, modification-dependent protein binding, damaged DNA binding, helicase activity, ATP-dependent 3′-5′ DNA helicase activity, and single-stranded DNA binding (Figure 3A, 3B, and 3E). GO analysis suggested that pressure overload significantly promoted cardiomyocyte proliferation.

KEGG Pathway Analysis Showed That Most Enriched Terms Were Closely Related to Cell Proliferation

We performed KEGG pathway analysis to find out whether the pathways regulating differentially

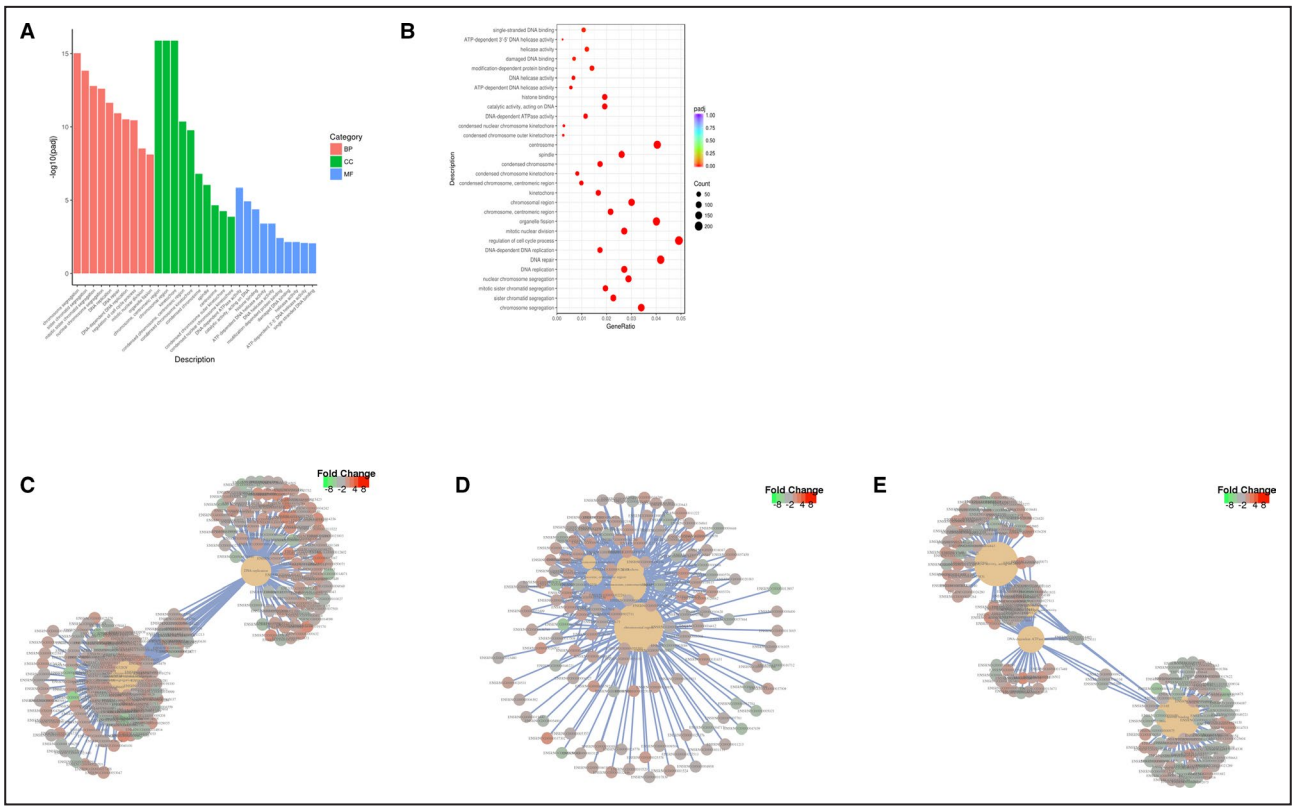

Figure 3. GO analysis indicates that the differentially expressed genes mainly mediate mitosis and cell division.
A, From the results of the GO enrichment analysis, the most significant 30 terms are displayed. The abscissa is the GO Term, and the ordinate is the significance level of GO Term enrichment. The higher the value, the more significant, and the different colors represent 3 different GO subclasses: biological process (BP), (CC), and MF. **B**, From the results of the GO enrichment analysis, we selected the most significant 30 terms to draw scatterplots for display. The abscissa is the ratio of the number of differentially expressed genes on the GO Term to the total number of differentially expressed genes, the ordinate is the GO Term, the size of the dots represents the number of genes annotated to the GO Term, and the color from red to purple represents the significance level of GO Term enrichment. **C**, A network diagram of the top 5 most significant GO Terms in BP. **D**, A network diagram of the top 5 most significant GO Terms in BP in MF in CC. **E**, A network diagram of the top 5 most significant GO Terms in biological processes in molecular functions. BP indicates biological processes; CC, cellular components; GO, gene ontology; and MF, molecular function.

expressed genes were associated with cell proliferation. The top 10 enriched pathways were cell cycle, DNA replication, nucleotide excision repair, mismatch repair, small cell lung cancer, pyrimidine metabolism, homologous recombination, base excision repair, bladder cancer, and Fanconi anemia pathway (Figure 4A through C). KEGG pathway analysis suggested that pressure overload largely activated pathways associated with cell proliferation.

Verification of RNA-seq Results by Proliferation Marker Detection

To confirm the RNA-seq results, we performed immunostaining on both PAB rat model samples at P7 and on human samples of pressure-overloaded RVs (Table). The number of Ki67-positive cardiomyocytes per section was 262.9±15.1 in the PAB group and 182.1±14.4 in the sham group (Figure 5A and 5B). The number of pH3-positive cardiomyocytes was 66.4±5.9 in the PAB group and 45.3±4.9 in the sham group (Figure 5C and 5D). The percentage of pH3-positive cardiomyocytes in sham and PAB groups was 0.412%±0.162% and 1.585%±0.223%, respectively (P<0.0001, n=10), and the percentage of Ki67-positive cardiomyocytes in sham and PAB was 2.563%±0.381% and 7.628%±1.468%, respectively (P<0.0001, n=10) (Figure S4). The number of aurora B-positive cardiomyocytes was 3.8±0.9 in the PAB group and 0.4±0.5 in the sham group (Figure 5E and 5F). In addition to immune staining, we also used synthetic nucleoside uptake to confirm the above results. As shown in Figure S5, at P7 the number of EdU-positive cardiomyocytes per section was 555.9±64.6 in the PAB group and 286±53.8 in the sham group.

In the human RV samples, the number of Ki67-positive cardiomyocytes per section in the non-overload group was 14.6±3.5 and in the overload group it was 30±3.2 (P<0.0001, Figure 5G and 5I). The number of pH3-positive cardiomyocytes per section in the non-overload group was 4.3±1.4 and in the overload group it was 10.5±2.1 (P<0.0001, Figure 5H and 5I). The number of aurora B-positive cardiomyocytes was 1.5±0.5 in the overloaded group while there were none observed in the nonoverload group (Figure 5J and 5K). RNA-seq data (GSE139561) showed that the average fragments per kilobase of transcript sequence per million of AURKB in the PAB group was 9.54±1.07 and in the sham group it was 4.21±0.42. qRT-PCR results showed that the relative mRNA level of AURKB increased ≈10-fold (Figure S2).

These results suggested that pressure overload indeed profoundly promoted and extended the rate of the proliferation of RVCMs both in humans and rats.

Effect of Pressure Overload on RVCM Proliferation Diminishes With Age

Another important issue is the age-associated proliferation ability of cardiomyocytes.[11,23] We examined the proliferation status of cardiomyocytes at P3 and P14. We found that the number of Ki67-positive RVCMs in the sham group at P3, P7, and P14 was 205.6±20.6, 182.1±14.4, and 26.8±2.7, respectively, and the number of pH3-positive RVCMs in the sham group at P3, P7, and P14 was 54±6.3, 45.3±4.9, and 13.6±1.7, respectively (Figure 6A through C). When these RVCMs were subjected to pressure overload, we found that the Ki67-fold change (relative to the sham group) at P3, P7, and P14 was 2.4±0.2, 1.5±0.2, and 1.1±0.2, respectively, and

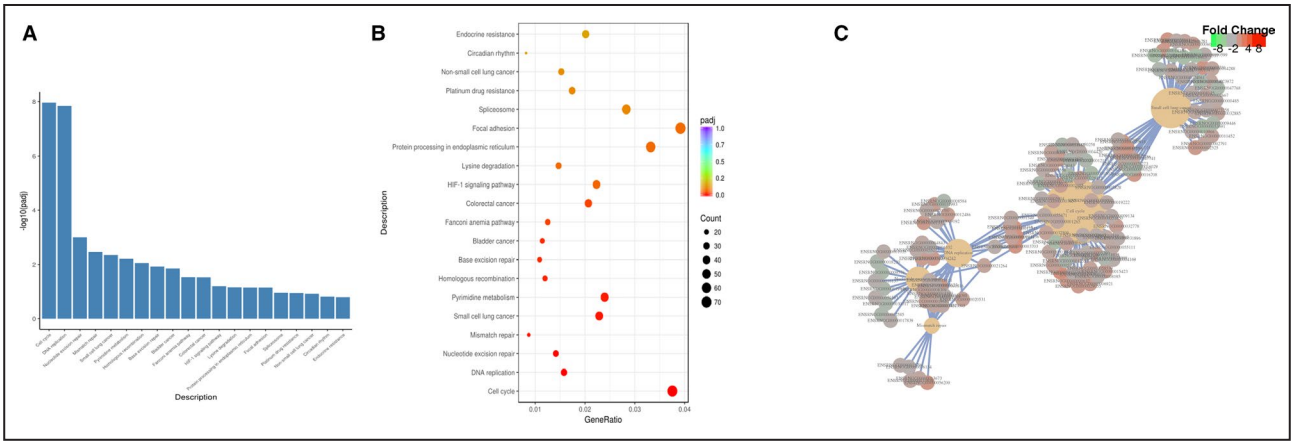

Figure 4. KEGG pathway analysis indicates that the differentially expressed genes mainly mediate mitosis and cell division. **A**, From the KEGG enrichment results, the most significant 20 KEGG pathways are displayed. The abscissa is the KEGG pathway, and the ordinate is the significance level of pathway enrichment. The higher the value, the more significant. **B**, From the KEGG enrichment results, the most significant 20 KEGG pathways were selected for the scatterplots. The abscissa is the ratio of the number of differentially expressed genes on the KEGG pathway to the total number of differentially expressed genes, the ordinate is the KEGG pathway, the size of the dots represents the number of genes annotated to the KEGG pathway, and the color from red to purple the represents significance level of KEGG pathway enrichment. **C**, The Network of the top 5 most significantly enriched KEGG pathways. KEGG indicates Kyoto Encyclopedia of Genes and Genomes.

Table. Patients' Clinical Information

Group	Sampling Date	Age (mo)	Sex	Body Weight (kg)	Right Ventricle Pressure Load (mm Hg)	SaO_2 (%)
Nonoverload	2015/3/20	2.2	Male	4.5	10.96	89
	2015/6/23	3	Male	6	20.6	98
	2015/8/24	2.3	Female	5.4	28.5	63
	2016/3/29	3	Male	6.2	21.4	69
	2016/5/25	2.5	Female	7.5	18.6	89
	2016/7/8	2.3	Female	8	17.7	87
	2017/11/30	2.4	Female	7.3	27.5	73
	2018/4/3	3	Male	5.7	16.7	98
	2018/4/17	3	Male	7	26.8	77
	2018/7/6	3	Male	6.2	26.4	78
Pressure overload	2015/3/6	3	Male	4.8	70	80
	2015/4/7	2.5	Male	6	114	88
	2015/9/8	3	Male	6.1	64	88
	2016/1/14	2.8	Female	7.3	96	80
	2016/3/11	2.1	Male	6.6	70.9	80
	2016/4/12	3	Male	5.8	73	88
	2017/5/18	2.9	Male	6.5	65	87
	2017/6/16	3	Male	5	186.1	85
	2018/3/19	3	Male	7.1	64	87
	2018/5/21	3	Male	7.5	88	86

SaO_2 indicates arterial oxygen percent saturation.

the pH3-fold change at P3, P7, and P14 was 2.3±0.6, 1.5±0.2, and 1.0±0.2, respectively (Figure 6A through C). EdU uptake experiments showed that the number of EdU-positive RVCMs in the sham group at P3, P7, and P14 was 498.5±63.1, 286±53.8, and 193.7±30.4, respectively, and in the PAB group at P3, P7, and P14 were 826±72.8, 555.9±64.6, and 251.6±30.4, respectively (Figure S5). These data demonstrate that the effects of pressure overload on the promotion of RVCM proliferation diminish with age.

Cardiomyocyte Hypertrophy Without RV Fibrosis in the Pressure Overload Model

At the adult stage, pressure overload induces RVCMs hypertrophy, but how pressure overload affects neonatal RVCMs is largely unknown. We found that cell size increased 42% (Figure 7A and 7B), and cardiac hypertrophy markers atrial natriuretic peptide and brain natriuretic peptide increased 33.3-fold and 16.5-fold, respectively (Figure 7C).

Fibrosis is an important feature of both the apex resection model and the myocardial infarction model. Therefore, we investigated fibrosis in the pressure overload model. Fibrosis was undetectable (Figure 7D) in the pressure overload model. The expression levels of markers such as collagen type I alpha 1, collagen type III alpha 1, and type II and type IV collagen had no change between the PAB and sham groups at P7 (Figure 7E through G).

These results suggest that cardiomyocyte hypertrophy, but not fibrosis, is a feature of the pressure overload model.

DISCUSSION

A good disease model is critical for disease research. Current animal models for heart regeneration studies are controversial. Since 2011, when Porrello et al reported a 7-day transient regenerative potential of the neonatal mouse heart,[25] heart regeneration results have always been challenged. Andersen et al followed an apex resection model for 180 days and found persistent scarring and dilated cardiomyopathy,[7] suggesting there was no regeneration. Bryant et al performed a systematic analysis of an apical resection model and found that the sizes of the cardiac resection and the surgical retraction of the ventricular apex both played critical roles in the resection model.[10] Even more recently, Notari et al reported that only 1-day-old neonatal mice had regenerative potential, but that 2-day-old mice responded to amputation with fibrosis rather than regeneration.[26] When considering a myocardial infarction model, Haubner et al reported that there was only a very limited set of differentially expressed genes between sham operation and myocardial infarction heart tissue.[11] Quaife-Ryan et al did multicellular transcriptional analysis on the regenerative heart and

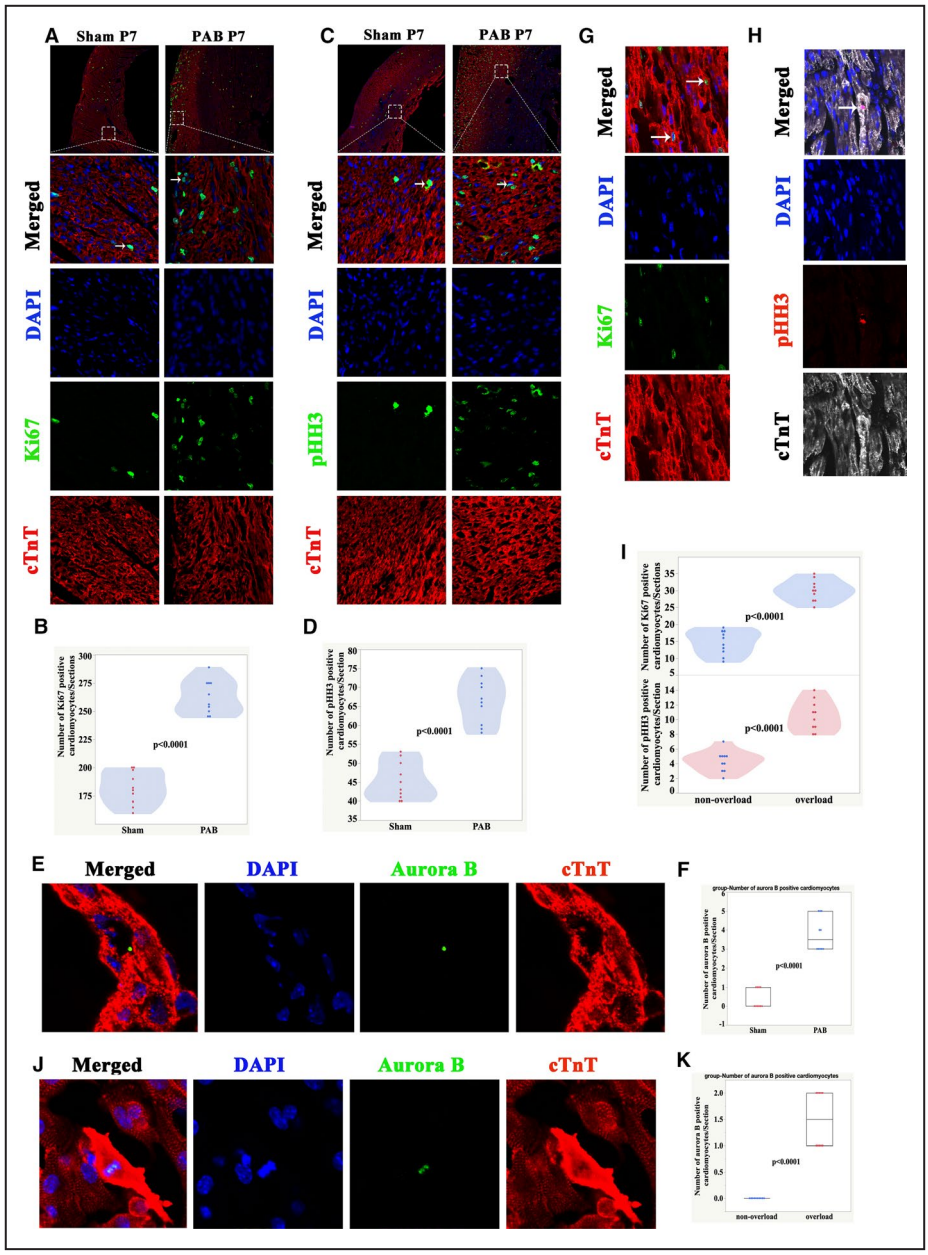

Figure 5. Immunofluorescence staining confirms that pressure overload greatly promotes RVCM proliferation.

A, Immunofluorescence staining for Ki67 (green), cardiac troponin T (red), and DAPI (blue) in rats at P7. **B**, Quantification of Ki67-positive cardiomyocytes at P7, n=10 samples. **C**, Immunofluorescence staining for pHH3 (green), cTnT (red), and DAPI (blue) in rats at P7. Arrows indicate proliferating cardiomyocytes. **D**, Quantification of pHH3-positive cardiomyocytes, n=10 samples. **E**, Immunofluorescence staining for aurora B (green), cTnT (red), and DAPI (blue) in rats at P7. **F**, Quantification of aurora B-positive cardiomyocytes at P7. **G**, Representative Ki67-positive cardiomyocytes from patients with RV pressure overload. Ki67 (green), cardiac troponin T (red), and DAPI (blue). Arrows indicate proliferating cardiomyocytes. **H**, Representative pHH3-positive cardiomyocytes from patients with RV pressure overload. pH3 (red), cTnT (white), and DAPI (blue). Arrows indicate proliferating CMs. **I**, Quantification of Ki67/pHH3-positive cardiomyocytes in human samples. **J**, Representative Ki67-positive cardiomyocytes from patients with RV pressure overload. Aurora B (green), cTnT (red), and DAPI (blue). **K**, Quantification of aurora B-positive cardiomyocytes in human samples. CMs indicates cardiomyocytes; cTnT, cardiac troponin T DAPI, 4′,6-diamidino-2-phenylindole; PAB, pulmonary artery banding; pHH3, phospho-histone H3; RV, right ventricle; and RVCM, right ventricular cardiomyocyte.

found that the majority of transcriptional changes in all of the cardiac cell types resulted from developmental maturation from neonatal stages to adulthood rather than activation of a distinct regeneration-specific gene program.[9] The above findings question the suitability of apex resection and myocardial infarction models for heart regeneration studies. The adult myocardial infarction model is used for the understanding the pathophysiological processes of adult myocardial infarction patients. Here, we present a new model of heart regeneration. Our RNA-seq data showed that there were >5000 genes that were differentially expressed. GO and KEGG pathway analysis suggested that most of these differentially expressed genes were involved in mitosis and cell division. These results suggest that, compared with apex resection models and myocardial infarction models, the pressure overload model is much better.

Another interesting feature of the pressure overload model is that pressure overload extends the time frame of cardiomyocyte proliferation. Usually at P7, cardiomyocyte gene programs change from proliferation to maturation and hypertrophy. Our results showed that at P7 there were still many proliferating genes that were active. However, it should be noted that the proliferative activity of RVCMs diminished with time, and hypertrophy was inevitable. This suggested that PAH (pulmonary artery hypertension) cannot change the exit of cell cycle of RVCM. It is better to perform the PAB model to study heart regeneration before P7.

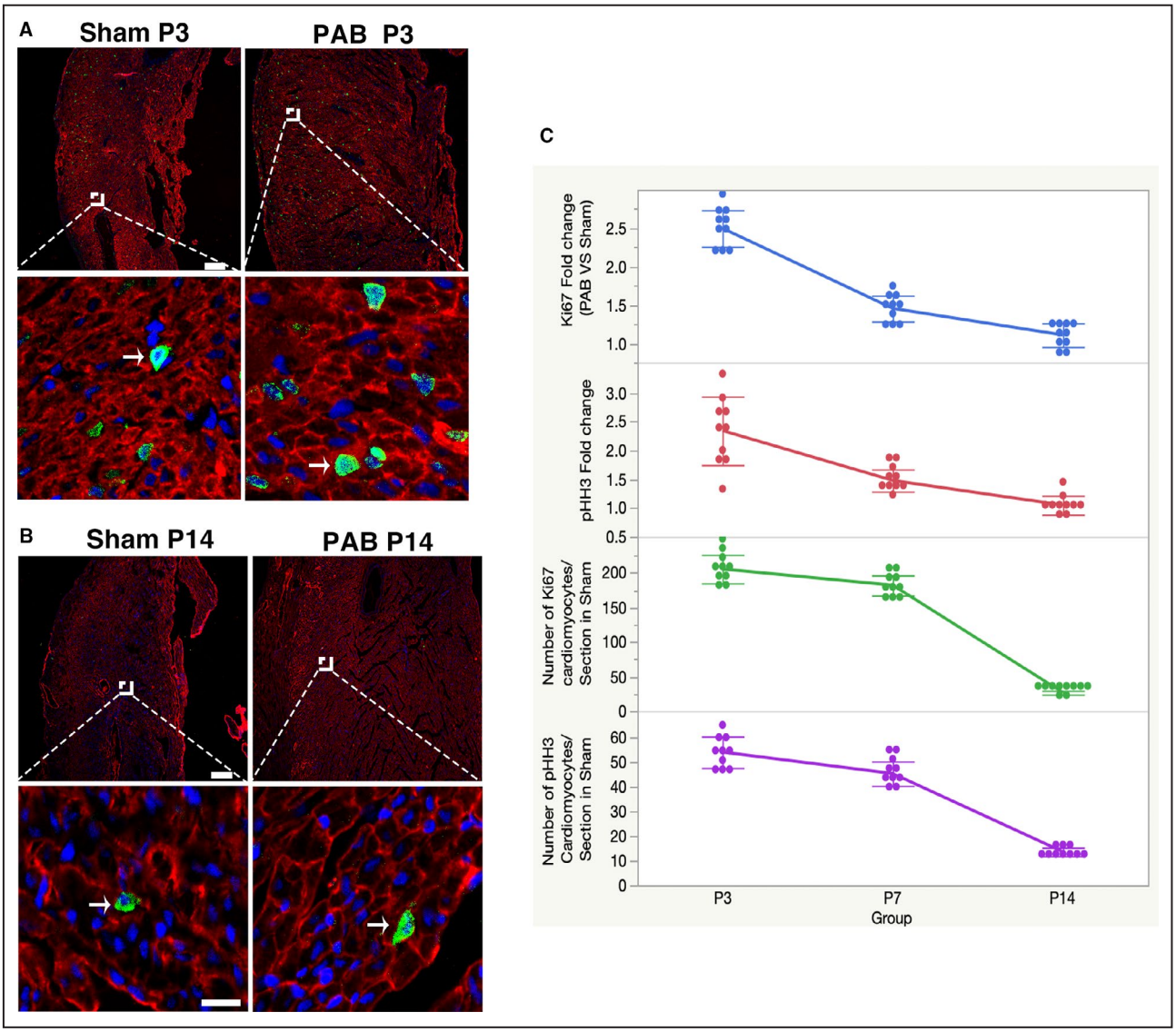

Figure 6. Pressure overload promotes RVCM proliferation associated with rat age.
Dash LINE indicates scale bar. **A**, 25 μm; **B**, 100 μm, above panel. Arrow indicates proliferating CMs. **A**, Immunofluorescence staining for Ki67 (green), cardiac troponin T (red), and DAPI (blue) in rats at P3. **B**, Immunofluorescence staining for pH3 (green), cardiac troponin T (red), and DAPI (blue) in rats at P14. **C**, Quantification of Ki67/pHH3-positive cardiomyocytes at different ages. DAPI indicates 4′,6-diamidino-2-phenylindole; PAB, pulmonary artery banding; pHH3, phospho-histone H3; and RVCM, right ventricular cardiomyocyte.

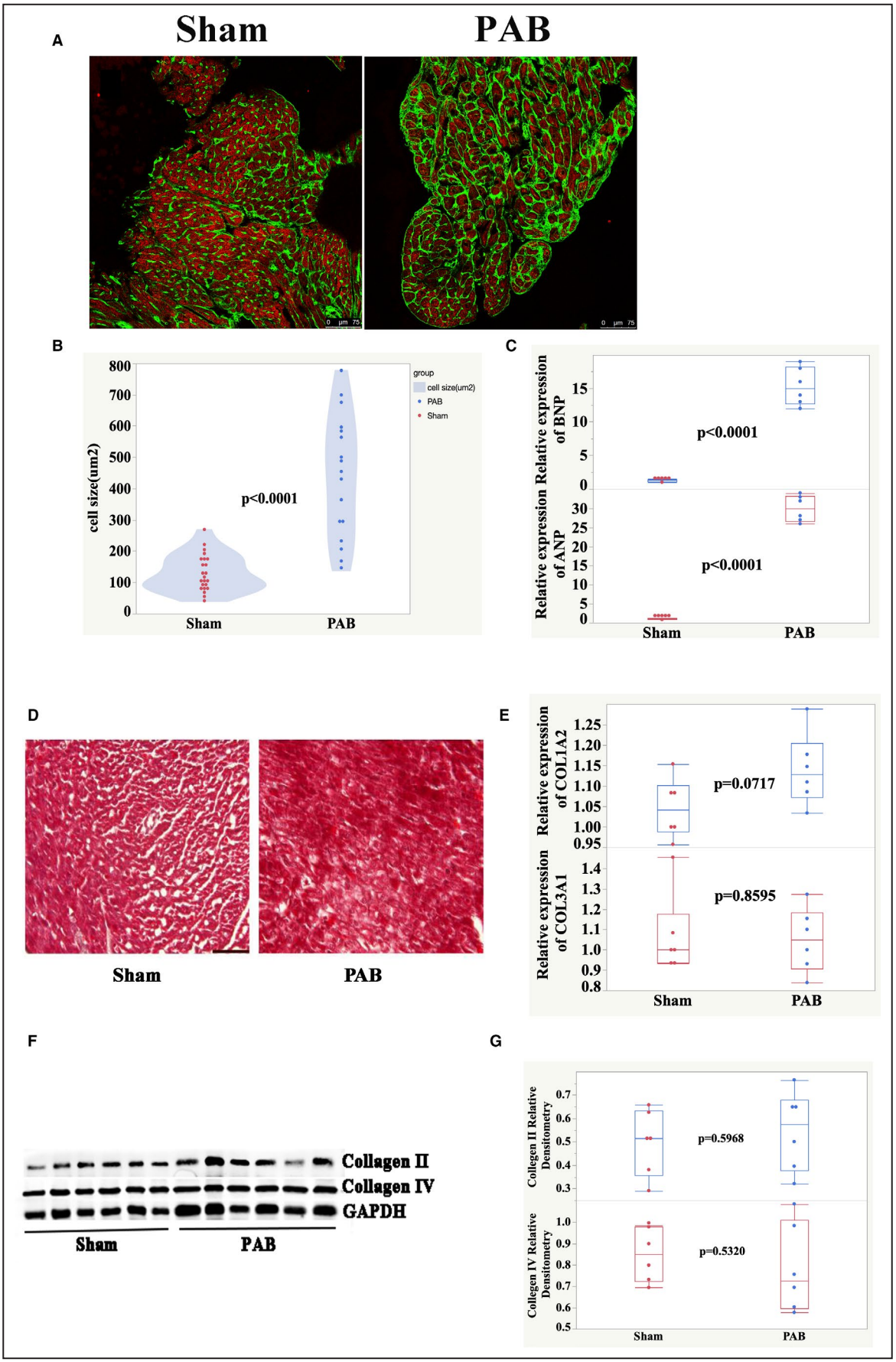
A
Sham
PAB
B
cell size(um2)
group
cell size(um2)
PAB
Sham
p<0.0001
Sham
PAB
C
Relative expression of BNP
p<0.0001
Relative expression of ANP
p<0.0001
Sham
PAB
D
Sham
PAB
E
Relative expression of COL1A2
p=0.0717
Relative expression of COL3A1
p=0.8595
Sham
PAB
F
Collagen II
Collagen IV
GAPDH
Sham
PAB
G
Collegen II Relative Densitometry
p=0.5968
Collegen IV Relative Densitometry
p=0.5320
Sham
PAB

Figure 7. Cardiomyocytes hypertrophy without fibrosis in pressure overload model.
A, Heart sections were stained with Alexa 488-conjugated WGA (green), cardiac troponin T (red), and DAPI (blue). **B**, Quantification of cell size. **C**, qPCR analysis of mRNA expression levels for cardiac hypertrophy markers ANP and BNP. **D**, Trichrome green–stained sections of RV. Scale bar, 50 μm. **E**, qPCR analysis of mRNA expression levels for cardiac fibrosis markers Col1a2 and Col3a1. **F**, Detection of collagen II and IV from P7 rat hearts by Western blot. **G**, Quantification of Western blot bands from (**F**). ANP indicates atrial natriuretic peptide; BNP, brain natriuretic peptide; DAPI, 4′,6-diamidino-2-phenylindole; PAB, pulmonary artery banding; qPCR, quantitative real-time polymerase chain reaction; and RV, right ventricle.

An exciting result revealed by Malek et al showed that pressure overload induces left ventricular cardiomyocyte proliferation.[13] However, that study did not compare sham and operated cardiomyocytes by RNA-seq at P7, so we do not know what transcriptomic changes existed between their sham and operated cardiomyocytes. Combined with their study, we conclude that pressure overload is able to induce the whole heart to proliferate at the neonatal stage. This may mean that we are able to induce cardiomyocyte proliferation at the prenatal stage by pressure overload, since minimally invasive prenatal surgery is becoming more common.[17]

In clinical practice, many congenital heart diseases, such as pulmonary stenosis, tetralogy of Fallot, double-outlet RV, transposition of the great arteries, and others, have RV overload right after birth. Little is known about how the neonatal RV responds to pressure and/or volume overload. Previous studies have applied monocrotaline or chronic hypoxia to induce pulmonary hypertension that increases RV afterload.[27,28] Those methods take at least 1 week to establish pulmonary hypertension. Hence, they are unlikely to be useful for studying RV remodeling right after birth. Here, we established a neonatal RV overload rat model by constricting the main pulmonary artery at P1. With this system, we can model the pathogenesis of many congenital heart diseases. Since there are many children with congenital heart disease with RV or left ventricle overload, this will make it easier to test the results of the pressure overload model on human beings than would the apex resection model or myocardial infarction model.

In summary, we present a new model for heart regeneration studies. If we take cardiomyocyte proliferation as the main index, this model is much better than the controversial apex resection and myocardial infarction models. In clinical practice, there are many children with congenital heart disease with pressure overload, which makes our model more attractive for medical translational purposes.

ARTICLE INFORMATION

Received December 16, 2019; accepted May 4, 2020.

Affiliations

From the Departments of Thoracic and Cardiovascular Surgery (L.Y., S.W., Y.X., C.J., H.C., H.Z., H.Z., J.L., Z.X.) and Anesthesiology (Y.H.), Institute of Pediatric Translational Medicine (L.Y., C.J., H.H.), Shanghai Institute for Pediatric Congenital Heart Disease (L.Y., C.J., H.Z.), Department of Plastic and Reconstructive Surgery, Shanghai Ninth People's Hospital, Shanghai Jiao Tong University School of Medicine, Shanghai, China (S.W.)

Sources of Funding

This work was supported by the National Natural Science Foundation of China (Nos. 81670287 and 81800285), National Key R&D Program of China (No. 2019YFA0110401), Foundation of Pudong Science and Technology Development (No. PKJ2016-Y35 and PKJ2019-Y12), Foundation of Shanghai Health and Family Planning Committee (No. 20164Y0106), Program for Outstanding Medical Academic Leader in Shanghai (Hao Zhang), and National Basic Research Program of China (No. 2013CB945304).

Disclosures

None.

Supplementary Materials

Tables S1–S4
Figures S1-S5

REFERENCES

1. Shudo Y, Wang H, Lingala B, He H, Kim FY, Hiesinger W, Lee AM, Boyd JH, Currie M, Woo YJ. Evaluation of risk factors for heart-lung transplant recipient outcome: an analysis of the united network for organ sharing database. *Circulation*. 2019;140:1261–1272.
2. Zhang Y, Zhang J, Butler J, Yang X, Xie P, Guo D, Wei T, Yu J, Wu Z, Gao Y, et al. Contemporary epidemiology, management, and outcomes of patients hospitalized for heart failure in China: results from the China Heart Failure (China-HF) Registry. *J Card Fail*. 2017;23:868–875.
3. Schüttler D, Clauss S, Weckbach LT, Brunner S. Molecular mechanisms of cardiac remodeling and regeneration in physical exercise. *Cells*. 2019;8:1128.
4. Morikawa Y, Heallen T, Leach J, Xiao Y, Martin JF. Dystrophin-glycoprotein complex sequesters Yap to inhibit cardiomyocyte proliferation. *Nature*. 2017;547:227–231.
5. Wang Z, Cui M, Shah AM, Ye W, Tan W, Min YL, Botten GA, Shelton JM, Liu N, Bassel-Duby R, et al. Mechanistic basis of neonatal heart regeneration revealed by transcriptome and histone modification profiling. *Proc Natl Acad Sci USA*. 2019;116:18455–18465.
6. Fan Q, Mao H, Angelini A, Coarfa C, Robertson MJ, Lagor WR, Wehrens XHT, Martin JF, Pi X, Xie L. Depletion of endothelial prolyl hydroxylase domain protein 2 and 3 promotes cardiomyocyte proliferation and prevents ventricular failure induced by myocardial infarction. *Circulation*. 2019;140:440–442.
7. Andersen DC, Jensen CH, Baun C, Hvidsten S, Zebrowski DC, Engel FB, Sheikh SP. Persistent scarring and dilated cardiomyopathy suggest incomplete regeneration of the apex resected neonatal mouse myocardium–a 180 days follow up study. *J Mol Cell Cardiol*. 2016;90:47–52.
8. Cai W, Tan J, Yan J, Zhang L, Cai X, Wang H, Liu F, Ye M, Cai CL. Limited regeneration potential with minimal epicardial progenitor conversions in the neonatal mouse heart after injury. *Cell Rep*. 2019;28:190–201.e3.
9. Quaife-Ryan GA, Sim CB, Ziemann M, Kaspi A, Rafehi H, Ramialison M, El-Osta A, Hudson JE, Porrello ER. Multicellular transcriptional analysis of mammalian heart regeneration. *Circulation*. 2017;136:1123–1139.
10. Bryant DM, O'Meara CC, Ho NN, Gannon J, Cai L, Lee RT. A systematic analysis of neonatal mouse heart regeneration after apical resection. *J Mol Cell Cardiol*. 2015;79:315–318.

11. Haubner BJ, Adamowicz-Brice M, Khadayate S, Tiefenthaler V, Metzler B, Aitman T, Penninger JM. Complete cardiac regeneration in a mouse model of myocardial infarction. *Aging (Albany NY)*. 2012;4:966–977.
12. Hoog TG, Fredrickson SJ, Hsu CW, Senger SM, Dickinson ME, Udan RS. The effects of reduced hemodynamic loading on morphogenesis of the mouse embryonic heart. *Dev Biol*. 2018;442:127–137.
13. Malek Mohammadi M, Abouissa A, Azizah I, Xie Y, Cordero J, Shirvani A, Gigina A, Engelhardt M, Trogisch FA, Geffers R, et al. Induction of cardiomyocyte proliferation and angiogenesis protects neonatal mice from pressure overload-associated maladaptation. *JCI Insight*. 2019;5:e128336.
14. Downing TE, Kim YY. Tetralogy of Fallot: general principles of management. *Cardiol Clin*. 2015;33:531–541, vii-viii.
15. Vriz O, Pirisi M, Bossone E, Fadl ElMula FEM, Palatini P, Naeije R. Right ventricular-pulmonary arterial uncoupling in mild-to-moderate systemic hypertension. *J Hypertens*. 2020;38:228–274.
16. Driessen MM, Hui W, Bijnens BH, Dragulescu A, Mertens L, Meijboom FJ, Friedberg MK. Adverse ventricular-ventricular interactions in right ventricular pressure load: insights from pediatric pulmonary hypertension versus pulmonary stenosis. *Physiol Rep*. 2016;4:e12833.
17. Graves CE, Harrison MR, Padilla BE. Minimally invasive fetal surgery. *Clin Perinatol*. 2017;44:729–751.
18. Spray TL, Mallory GB, Canter CB, Huddleston CB. Pediatric lung transplantation. Indications, techniques, and early results. *J Thorac Cardiovasc Surg*. 1994;107:990–999; discussion 999–1000.
19. Reddy S, Zhao M, Hu D-Q, Fajardo G, Hu S, Ghosh Z, Rajagopalan V, Wu J-C, Bernstein D. Dynamic microRNA expression during the transition from right ventricular hypertrophy to failure. *Physiol Genomics*. 2011;44:562–575.
20. Hsu DT, Zak V, Mahony L, Sleeper LA, Atz AM, Levine JC, Barker PC, Ravishankar C, McCrindle BW, Williams RV, et al. Enalapril in infants with single ventricle: results of a multicenter randomized trial. *Circulation*. 2010;122:333–340.
21. Wang S, Ye L, Hong H, Tang C, Li M, Zhang Z, Liu J. A neonatal rat model of increased right ventricular afterload by pulmonary artery banding. *J Thorac Cardiovasc Surg*. 2017;154:1734–1739.
22. Ye L, Qiu L, Zhang H, Chen H, Jiang C, Hong H, Liu J. Cardiomyocytes in young infants with congenital heart disease: a three-month window of proliferation. *Sci Rep*. 2016;6:23188.
23. Polizzotti BD, Ganapathy B, Walsh S, Choudhury S, Ammanamanchi N, Bennett DG, dos Remedios CG, Haubner BJ, Penninger JM, Kühn B. Neuregulin stimulation of cardiomyocyte regeneration in mice and human myocardium reveals a therapeutic window. *Sci Transl Med*. 2015;7:281ra45.
24. Wang S, Ye L, Li M, Liu J, Jiang C, Hong H, Zhu H, Sun Y. GSK-3β inhibitor CHIR-99021 promotes proliferation through upregulating β-catenin in neonatal atrial human cardiomyocytes. *J Cardiovasc Pharmacol*. 2016;68:425–432.
25. Porrello ER, Mahmoud AI, Simpson E, Hill JA, Richardson JA, Olson EN, Sadek HA. Transient regenerative potential of the neonatal mouse heart. *Science*. 2011;331:1078–1080.
26. Notari M, Ventura-Rubio A, Bedford-Guaus SJ, Jorba I, Mulero L, Navajas D, Martí M, Raya Á. The local microenvironment limits the regenerative potential of the mouse neonatal heart. *Sci Adv*. 2018;4:eaao5553.
27. Weiss A, Neubauer MC, Yerabolu D, Kojonazarov B, Schlueter BC, Neubert L, Jonigk D, Baal N, Ruppert C, Dorfmuller P, et al. Targeting cyclin-dependent kinases for the treatment of pulmonary arterial hypertension. *Nat Commun*. 2019;10:2204.
28. Kurosawa R, Satoh K, Kikuchi N, Kikuchi H, Saigusa D, Al-Mamun ME, Siddique MAH, Omura J, Satoh T, Sunamura S, et al. Identification of celastramycin as a novel therapeutic agent for pulmonary arterial hypertension. *Circ Res*. 2019;125:309–327.

SUPPLEMENTAL MATERIAL

Table S1. Primer information.

Gene		Sequence (5' -> 3')
COL1A1	Forward	CTCAAGATGTGCCACTCTGACT
	Reverse	GAGGGAGTTTACAGGAAGCAGAC
COL3A1	Forward	TGGCGGCTTTTCACCATATT
	Reverse	ACTCTCTATTTGTCCGTTAACAGACTTG
AURKB	Forward	CAGTGGGACACCCGACATC
	Reverse	GTACACGTTTCCAAACTTGCC
CCND1	Forward	GATCGGGCATCACCTGAAAAA
	Reverse	TCGTCTGGTATCTTACCTACTCG
Mki67	Forward	ACGCCTGGTTACTATCAAAAGG
	Reverse	CAGACCCATTTACTTGTGTTGGA
Ccnd3	Forward	TACCCGCCATCCATGATCG
	Reverse	AGGCAGTCCACTTCAGTGC
Bnp	Forward	CCTCTTCCTGGCCTTTTGG
	Reverse	TGTGTTGGACACCGCACTGT
Anp	Forward	GCTGCAGACTCCGGCTTCT
	Reverse	ATCACTTGAGAGGTGGTCCCA
Rrm2	Forward	GCCGAGCTGGAAAGTAAAGC
	Reverse	TCATGGTACTCGATGGGAAAGA
Pclaf	Forward	ATGGTGCGGACTAAAGCAGAC
	Reverse	CCTCGATGAAACTGATGTCGAAT
Mcm6	Forward	GAGGAACTGATTCGTCCTGAGA
	Reverse	CAAGGCCCGACACAGGTAAG
LOC100359539	Forward	GGGGCGGTGATCTCTACAC
	Reverse	GGGAGTCGGACATTATTGACCA
TCF19	Forward	GGGGCGGTGATCTCTACAC
	Reverse	GGGAGTCGGACATTATTGACCA
Spc24	Forward	GCCTTCCGCGACATAGAGG
	Reverse	CCTGCTCCTTCGCATTGAGA
Ncaph	Forward	GTCCTCGAAGACTTTCCTCAGA
	Reverse	TGAAATGTCAATACTCCTGCTGG
Pbk	Forward	CCAAACATTGTTGGTTATCGTGC
	Reverse	GGCTGGCTTTATATCGTTCTTCT
Prim1	Forward	ATGGAGACGTTTGACCCCAC
	Reverse	CGTAGTTGAGCCAGCGATAGT
Smc2	Forward	TCTCAGGTTCGGGCTTCTAAT
	Reverse	CCTGTACTCTGGTGTTGTTGG
Plk4	Forward	AAGCTCGACACTTCATGCACC
	Reverse	GCATTTTCAGTTGAGTTGCCAG
Dynll1	Forward	AGAGATGCAACAGGACTCGGT
	Reverse	CCAGGTGGGATTGTACTTCTTG
Mastl	Forward	GACTGAGGAGGGCGTGAATAG
	Reverse	AGCTTGGACCTGATGAGTCATA
Oxct1	Forward	GTTGGTGGTTTTGGGCTATGT
	Reverse	AGACCATGCGTTTTATCTGCTT
Cavin2	Forward	CATCCGGGACAACTCACAGG
	Reverse	CAGCGTCTAGCATGTTCACCA
Tk1	Forward	GGGCAGATCCAGGTGATTCTC
	Reverse	TGTAGCGAGTGTCTTTGGCATA

Khdrbs1	Forward	GGAGCCAGAGAACAAGTACCT
	Reverse	CATGGCGTGAGTGAAGGAC
Dnmt1	Forward	AGGCGGCTCAAAGATTTGGAA
	Reverse	GCAGAAATTCGTGCAAGAGATTC
Top2a	Forward	ACCATTGCAGCCTGTAAATGA
	Reverse	GGGCGGAGCAAAATATGTTCC
Melk	Forward	TCTCCCAGTAGCATTCTGCTT
	Reverse	TGATCCAGGGATGGTTCAATAGA
Tuba1b	Forward	ACCTTAACCGCCTTATTAGCCA
	Reverse	CACCACGGTACAACAGGCA
Mms22l	Forward	TGGACACCTATCTGAACTTCCC
	Reverse	ATGCCATGACGGTGGAAAAAG
Uhrf1	Forward	GCCATACCCTCTTCGACTACG
	Reverse	GCCCCAATTCCGTCTCATCC

Table S2. Reagents.

Name	Company	Catalog No.
Triton X-100	Sigma-Aldrich	T9284
HBSS	ThermoFisher Scientific, Pittsburgh, PA, USA	14175103
DNase	Worthington, Lakewood, NJ, USA	9003-98-9
RNase	Worthington, Lakewood, NJ, USA	9001-99-4
paraformaldehyde(PFA)	Sigma-Aldrich	158127
4',6-diamidino-2-phenylindole(DAPI)	ThermoFisher Scientific)	D3571
EdU Kit	Invitrogen	C10337
PureLink RNA Micro Scale Kit	Life Technologies, Carlsbad, California, USA	12183016
PrimeScriptTM reagent kit	Takara Bio, Kusatsu, Japan	RR037A
SYBR Green Power Premix Kits	Applied Biosystems, Foster City, California	4368577
RIPA lysis buffer	Beyotime, Shanghai, China	P0013B
NEB Next® UltraTM RNA Library Prep Kit	NEB, USA	E7760
TruSeq PE Cluster Kit	Illumina	v3-cBot-HS

Table S3. Antibodies.

Name	Company	Catalog No.
cardiac troponin T	Abcam	ab8295
sarcomeric α-actinin	Abcam	ab9465
Ki67	Abcam	ab15580
phosphorylated histone H3	Milipore	06-570
aurora B	Abcam	ab2254
collagen IV	Abcam	ab6585

collagen II	Abcam	ab34712
GAPDH	Abcam	ab8245

Table S4. Top 24 upregulated genes.

gene_id	OWOP1	OWOP2	OWOP3	OWOP4	OWOP5	OWOP6	OWCON1
ENSRNOG00000016561	273.4829	231.5473	357.1895	353.1868	319.7178	278.3281	47.80062
ENSRNOG00000054286	683.7071	622.605	933.4951	561.2283	626.8788	538.7381	95.60125
ENSRNOG00000003703	919.6343	877.307	1083.575	828.5375	880.9144	850.5133	296.1931
ENSRNOG00000008450	520.9656	379.0515	623.3306	482.608	439.4913	351.1951	66.57944
ENSRNOG00000058288	211.8529	198.9592	209.1109	263.6805	230.8537	191.1266	69.14019
ENSRNOG00000029862	404.4465	316.448	450.2388	400.359	379.6046	322.5261	132.3053
ENSRNOG00000012051	691.4109	617.4595	837.4442	764.4317	733.1294	597.2706	262.0498
ENSRNOG00000015308	376.5204	300.1539	384.2038	338.6723	332.2747	272.3554	63.16511
ENSRNOG00000031993	816.5967	794.9791	995.528	897.4815	898.3009	870.8205	371.3084
ENSRNOG00000022325	1196.969	1234.061	1464.777	1285.745	1206.428	950.8548	444.7165
ENSRNOG00000011654	364.9648	346.4634	453.2404	373.749	437.5595	359.5569	163.0343
ENSRNOG00000011222	3485.943	2979.242	3413.811	2742.036	2752.858	2569.458	1438.287
ENSRNOG00000054474	285.0385	238.408	297.1576	310.8527	251.1379	222.1847	84.50467
ENSRNOG00000043094	7277.148	8242.226	8049.269	6368.248	6687.029	4183.283	1916.293
ENSRNOG00000025895	4321.8	4195.294	4551.414	5081.293	4689.517	4191.645	2407.956
ENSRNOG00000047314	1208.525	899.6042	1207.641	918.0437	1083.757	973.5511	392.648
ENSRNOG00000046794	2315.938	2319.761	2327.234	2371.915	2237.059	2236.181	1678.997
ENSRNOG00000039859	1518.6	1354.981	1645.873	1331.708	1453.702	1380.89	704.2056
ENSRNOG00000053047	3165.275	2788.859	2936.558	2590.843	2705.528	2094.031	1224.037
ENSRNOG00000013598	268.668	212.6805	299.1587	258.8424	225.0582	236.5192	72.55452
ENSRNOG00000053468	11191.61	9963.395	12668.72	11016.52	10956.37	8328.341	4733.115
ENSRNOG00000006996	376.5204	367.9029	479.2542	445.1121	372.8432	352.3897	114.3801
ENSRNOG00000005659	854.1524	689.4964	891.4728	783.7844	747.6182	677.3049	365.3333
ENSRNOG00000048411	723.1888	610.5988	793.4208	576.9524	738.9249	659.3867	194.6168

OWCON2	OWCON3	OWCON4	OWCON5	OWCON6	Opt1w	Con1w	log2FoldCh	pvalue
53.82467	49.06721	49.1797	58.37299	39.2052	302.2421	49.57507	2.611407	1.05E-59
106.4532	99.22481	91.69096	127.8167	75.73733	661.1087	99.42071	2.737093	1.65E-59
267.9272	278.0475	265.0702	206.3183	211.1735	906.7469	254.1217	1.835709	2.31E-55
102.8649	71.96525	92.52451	89.57234	98.90404	466.107	87.06842	2.42227	2.78E-44
55.02077	55.60951	63.35012	54.34726	52.57062	217.5973	58.33974	1.891693	3.72E-43
123.1987	119.9421	105.8614	107.6881	98.90404	378.9372	114.6499	1.726325	9.30E-41
235.6324	240.9745	270.9051	266.7042	209.3914	706.8577	247.6096	1.512346	2.19E-40
77.74674	77.41716	41.67771	86.55305	51.67959	334.0301	66.37323	2.341963	9.86E-40
316.9675	432.8819	385.9356	387.4759	359.084	878.9511	375.6089	1.225466	2.25E-39
434.1857	444.8761	539.3095	459.9389	432.1483	1223.139	459.1958	1.412882	3.42E-37
147.1208	152.6536	160.876	140.9003	151.4747	389.2557	152.6766	1.348381	1.79E-36
1304.949	1286.651	1293.676	1200.672	1182.393	2990.558	1284.438	1.219458	3.38E-35
95.6883	85.04984	91.69096	94.6045	71.28219	267.4632	87.13674	1.62034	1.07E-34
1716.409	2039.015	1589.588	2066.202	1660.875	6801.201	1831.397	1.893055	1.07E-33
2285.754	2107.709	2629.03	2483.871	2344.293	4505.161	2376.436	0.922225	1.40E-32
391.1259	358.7358	290.0768	330.1093	240.5774	1048.52	333.8789	1.652762	2.28E-31
1560.915	1612.676	1508.733	1581.103	1579.792	2301.348	1587.036	0.536062	1.13E-30
810.9583	704.3871	721.8579	630.0257	609.4627	1447.625	696.8162	1.056133	1.58E-30
1246.34	1068.575	1017.77	1164.44	982.8032	2713.515	1117.328	1.280817	1.76E-30
64.5896	55.60951	89.1903	57.36656	42.76931	250.1545	63.67997	1.968585	6.51E-30
5069.088	5077.911	5079.679	4490.694	4429.297	10687.49	4813.297	1.150927	8.85E-30
133.9636	137.3882	116.6976	73.46945	82.86555	399.0037	109.7941	1.864984	1.70E-29
367.2038	288.9514	326.7532	377.4116	326.116	773.9715	341.9616	1.178754	4.78E-29
300.222	246.4264	225.8932	282.8071	201.3722	683.7454	241.8896	1.503354	1.52E-28

padj	gene_name	gene_chr	gene_start	gene_end	gene_stran	gene_length
1.55E-55	Pclaf	8	71514281	71526182	+	333
1.55E-55	Rrm2	6	43884678	43889515	+	1173
1.45E-51	Mcm6	13	45042882	45068077	-	2917
1.31E-40	LOC100359539	19	25391700	25394229	+	2530
1.41E-39	Tcf19	20	3744395	3746964	+	838
2.93E-37	Spc24	8	22780725	22785671	-	865
5.90E-37	Ncaph	3	1.2E+08	1.2E+08	-	2848
2.33E-36	Pbk	15	42489377	42500395	+	1830
4.71E-36	Prim1	7	2435553	2451165	+	1596
6.45E-34	Smc2	5	68717519	68763850	+	5373
3.07E-33	Plk4	2	1.28E+08	1.28E+08	+	3466
5.31E-32	Dynll1	12	47074200	47076572	+	652
1.56E-31	Mastl	17	89742140	89876825	+	5433
1.45E-30	Oxct1	2	53859737	54007756	+	3331
1.77E-29	Cavin2	9	55243255	55256340	-	3189
2.69E-28	Tk1	10	1.07E+08	1.07E+08	-	2218
1.25E-27	Khdrbs1	5	1.48E+08	1.48E+08	-	2622
1.65E-27	Dnmt1	8	21922515	21968495	-	5917
1.66E-27	Top2a	10	86901007	86932154	-	5589
5.85E-27	Melk	5	59783890	59844356	+	2842
7.60E-27	Tuba1b	7	1.41E+08	1.41E+08	-	1608
1.39E-26	Mms22l	5	38844488	38961035	+	4483
3.76E-26	Aurkb	10	55626741	55634991	+	4404
1.12E-25	Uhrf1	9	10738222	10757954	-	3856

gene_biotype	gene_description
protein_coding	PCNA clamp associated factor [Source:RGD Symbol;Acc:1303041]
protein_coding	ribonucleotide reductase regulatory subunit M2 [Source:RGD Symbol;Acc:15983
protein_coding	minichromosome maintenance complex component 6 [Source:RGD Symbol;Acc:
protein_coding	ribonucleotide reductase M2 polypeptide [Source:RGD Symbol;Acc:2323655]
protein_coding	transcription factor 19 [Source:RGD Symbol;Acc:1302974]
protein_coding	SPC24, NDC80 kinetochore complex component [Source:RGD Symbol;Acc:13076
protein_coding	non-SMC condensin I complex, subunit H [Source:RGD Symbol;Acc:1596799]
protein_coding	PDZ binding kinase [Source:RGD Symbol;Acc:1309565]
protein_coding	DNA primase subunit 1 [Source:RGD Symbol;Acc:621380]
protein_coding	structural maintenance of chromosomes 2 [Source:RGD Symbol;Acc:1305227]
protein_coding	polo-like kinase 4 [Source:RGD Symbol;Acc:1305390]
protein_coding	dynein light chain LC8-type 1 [Source:RGD Symbol;Acc:619866]
protein_coding	microtubule associated serine/threonine kinase-like [Source:MGI Symbol;Acc:M
protein_coding	3-oxoacid CoA transferase 1 [Source:RGD Symbol;Acc:1584008]
protein_coding	caveolae associated protein 2 [Source:RGD Symbol;Acc:1359345]
protein_coding	thymidine kinase 1 [Source:RGD Symbol;Acc:621014]
protein_coding	KH RNA binding domain containing, signal transduction associated 1 [Source:RGI
protein_coding	DNA methyltransferase 1 [Source:RGD Symbol;Acc:620979]
protein_coding	DNA topoisomerase II alpha [Source:RGD Symbol;Acc:62048]
protein_coding	maternal embryonic leucine zipper kinase [Source:RGD Symbol;Acc:1308974]
protein_coding	tubulin, alpha 1B [Source:RGD Symbol;Acc:1565476]
protein_coding	MMS22-like, DNA repair protein [Source:RGD Symbol;Acc:1304693]
protein_coding	aurora kinase B [Source:RGD Symbol;Acc:621625]
protein_coding	ubiquitin-like with PHD and ring finger domains 1 [Source:RGD Symbol;Acc:1595

10]
61967]

31]

GI:1914371]

D Symbol;Acc:621459]

855]

Figure S1. Flow cytometry indicates that ~99% of purified cells were cTnT- positive.

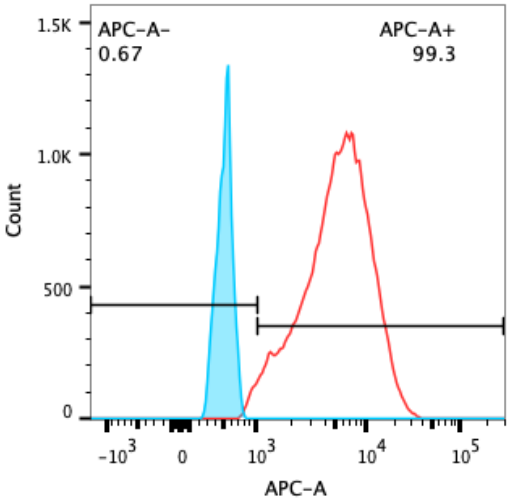

	Sample Name	Count
	Negtive control	14406
	Purified Sample	52780

Figure S2. qRT-PCR confirms the differentially expressed genes of RNA-seq data.

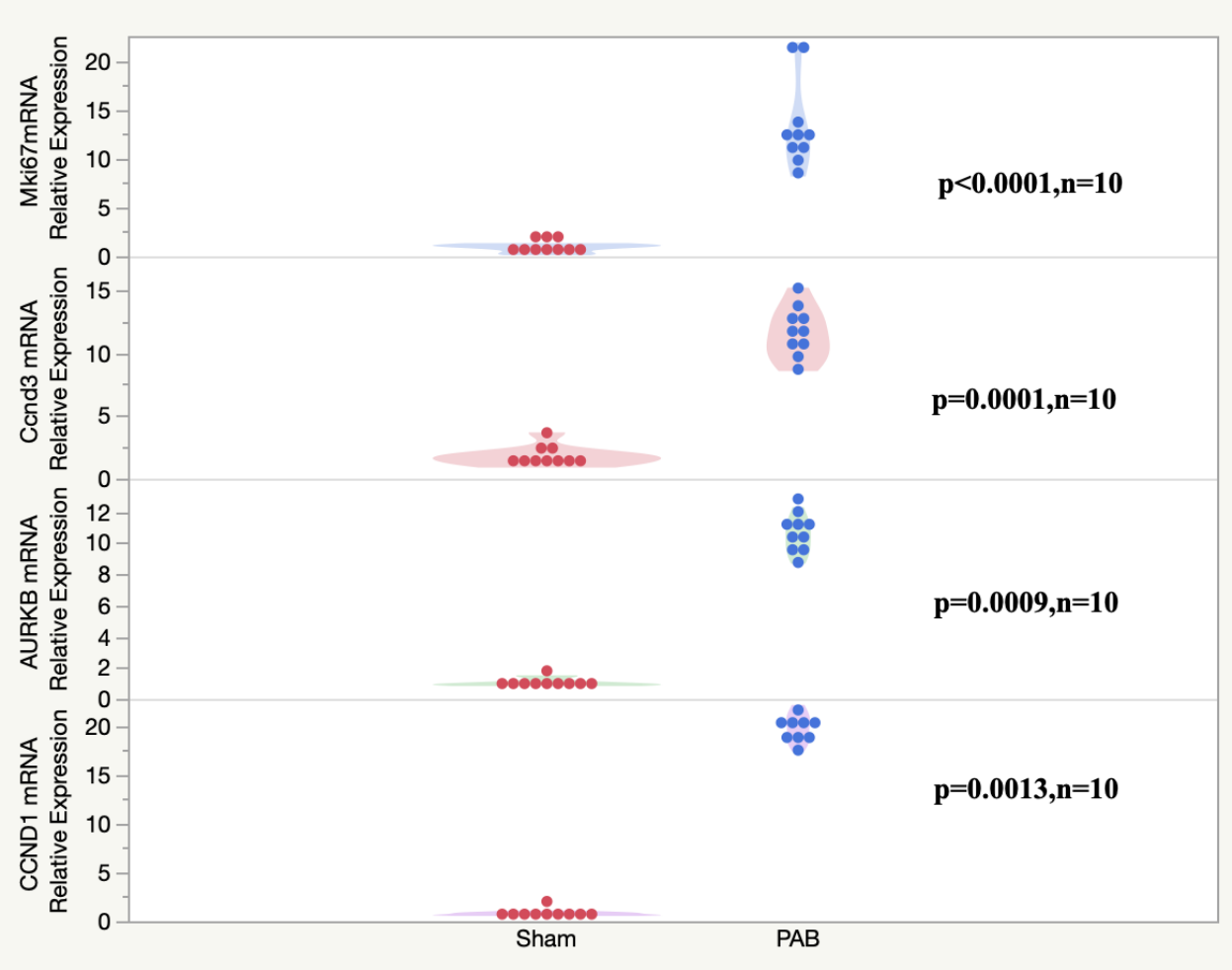

AURKB is one of the most important markers of cell division. RNA-seq data (GSE139561) showed that the average FPKM of *AURKB* in the PAB group was 9.54±1.07 and in the sham group was 4.21±0.42. Qrt-PCR results showed that the relative mRNA level of *AURKB* increased ~10 fold. RNA-seq data (GSE139561) showed that the average FPKM of *CCND1* in the PAB group was 22.8±6.2 and in the sham group was 7.78±1.12. qRT-PCR results showed that the relative mRNA level of *CCND1* increased ~20 fold. The other two cell cycle related genes *Mki67* and *Ccnd3* were also significantly increased.

Figure S3. The top 24 differentially expressed genes from RNA-seq data.

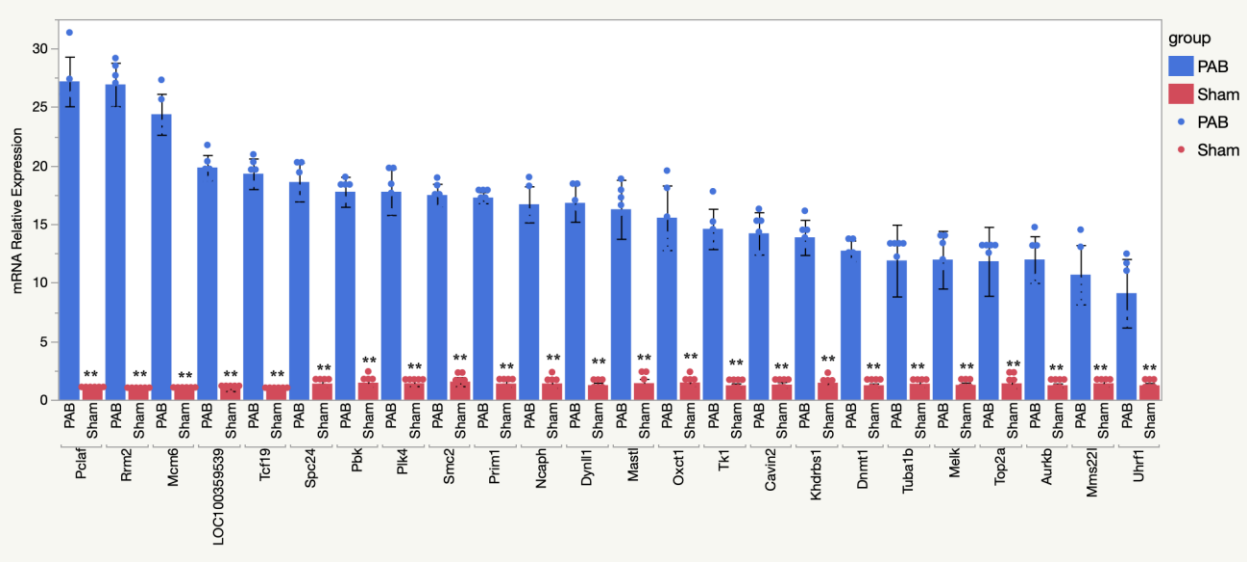

**P<0.01,n=10.

Figure S4 Quantification of the percentage of Ki67 and pH3 positive cardiomyocytes in sham and PAB rats at P7.

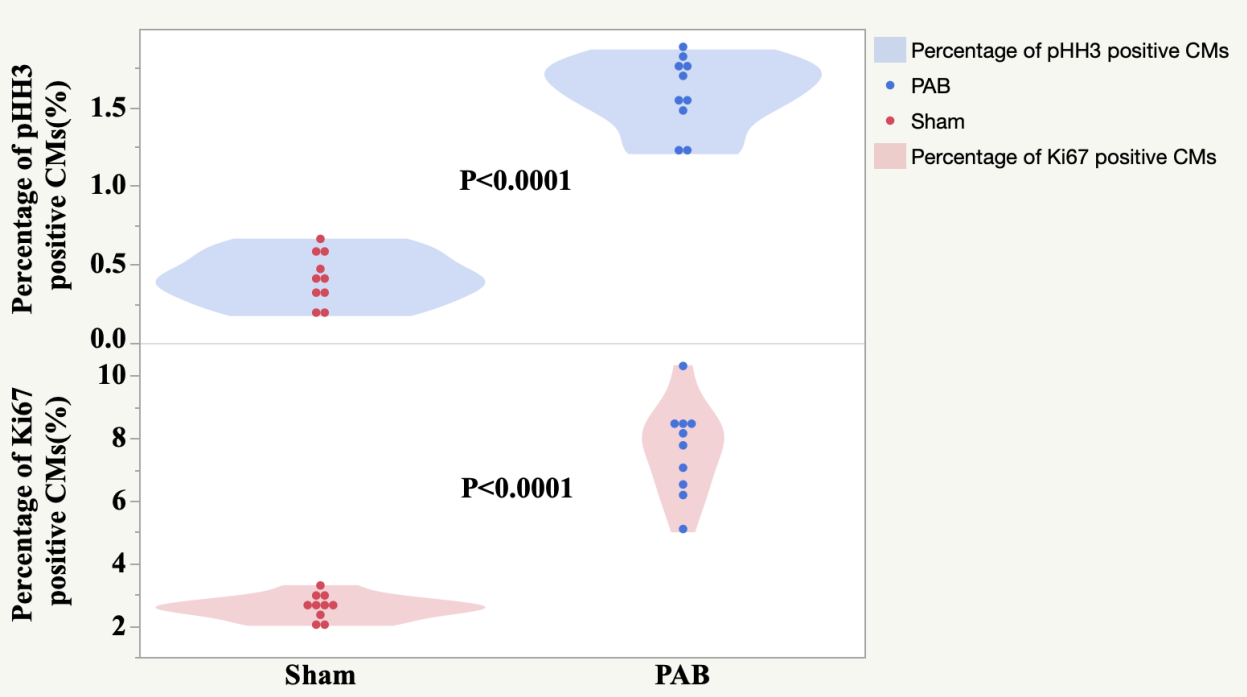

Figure S5. Nucleoside uptake confirms that pressure overload greatly promotes RVCM proliferation.

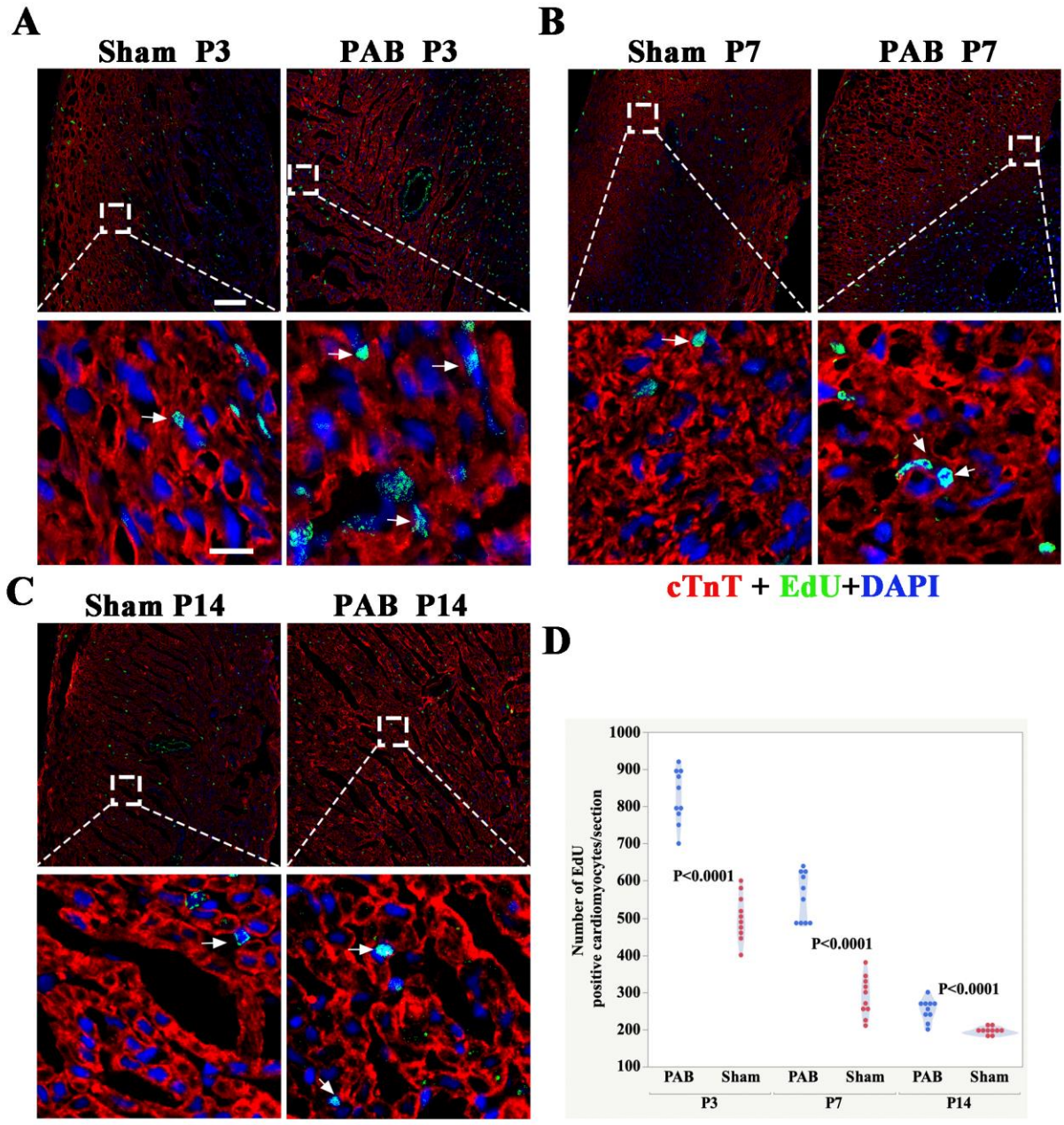

Representative graph of EdU-positive cardiomyocytes at P3(A), at P7(B), and at P14(C). (D) Quantification of EdU -positive cardiomyocytes at P7. Arrows indicate proliferating cardiomyocytes. EdU (green), cardiac troponin T (red) and DAPI (blue).